Applied Composite Materials (2022) 29:1715–1731
https://doi.org/10.1007/s10443-022-10038-z

A Novel Micromechanical Model Based on the Rule of Mixtures to Estimate Effective Elastic Properties of Circular Fiber Composites

Lucas L. Vignoli[1] · Marcelo A. Savi[2] · Pedro M. C. L. Pacheco[3] · Alexander L. Kalamkarov[4]

Received: 26 February 2022 / Accepted: 21 April 2022 /Published online: 18 May 2022
© The Author(s), under exclusive licence to Springer Nature B.V. 2022

Abstract
This paper proposes a novel model to estimate the effective elastic properties of unidirectional composites with circular cross section fibers: VSPKc. Finite element method (FEM) and experimental data are employed as reference solutions in order to verify the model capability to estimate the elastic properties. Experimental data considers a set of 126 tests compiled from the literature. In addition, predictions of two alternative analytical models are evaluated to highlight the advantages of the proposed model: the classical Rule of Mixtures (ROM) and a ROM-based model with octagonal cross section fibers. Results show that the VSPKc model presents the best estimations compared with either FEM or experimental data. The novel model highlights the importance of considering the fiber geometry on the estimation of elastic properties and establishes a simple set of closed-form formulas.

Keywords Micromechanics of composites · Effective elastic properties · Analytical modeling · Finite element method

✉ Marcelo A. Savi
savi@mecanica.coppe.ufrj.br

Lucas L. Vignoli
ll.vignoli@mecanica.coppe.ufrj.br

Pedro M. C. L. Pacheco
pedro.pacheco@cefet-rj.br

Alexander L. Kalamkarov
alex.kalamkarov@dal.ca

[1] Center for Technology and Applications of Composite Materials, Department of Mechanical Engineering, Universidade Federal Do Rio de Janeiro, Macaé, RJ, Brazil

[2] Center for Nonlinear Mechanics, COPPE – Department of Mechanical Engineering Universidade Federal Do Rio de Janeiro, 21.941.972, P.O. Box 68.503, Rio de Janeiro, Brazil

[3] Department of Mechanical Engineering, Centro Federal de Educação Tecnológica Celso Suckow da Fonseca CEFET/RJ, Rio de Janeiro, RJ, Brazil

[4] Department of Mechanical Engineering, Dalhousie University, Halifax, NS B3H 4R2, Canada

1 Introduction

Due to a large number of variables involved in the composite design [1], the analytical approaches are fundamental tools for the design and optimization procedures [2, 3]. Some applications highlighting the importance of micromechanical models for multiscale analysis are discussed for different structures as a pressure vessel [4] or notched plates [5, 6]. Composite materials have been applied in different scenarios to exploit their mechanical [7], thermal [8], chemical [9, 10] and dielectric [11] capabilities, as well as nanoscale technology [12, 13].

Micromechanical models can have a questionable accuracy due to unavoidable imperfections in the manufacturing process that include fiber nonuniform distribution [14] and the fiber surface influence on the fiber-matrix interface [15]. Ramos et al. [16] presented a discussion about interface modeling. On this basis, there are several research efforts to improve the accuracy of micromechanical modeling. In this regard, Vignoli et al. presented a general overview of micromechanical models to estimate the effective elastic properties and strength of composites, comparing with a large set of experimental data compiled from the literature [17–20].

In general, micromechanical models can be classified into three groups: models based on the Rule of Mixture (ROM-based); models based on the theory of elasticity; and trace-based models. The ROM-based models are usually based on simple assumptions of 2D elements (see Fig. 1) associated in series for the longitudinal elastic modulus, E_1, and in-plane Poisson's ratio, ν_{12}; or associated in parallel for transversal elastic modulus, E_2, in-plane shear modulus, G_{12}, and plane strain bulk modulus, K_{23} [21]. The out-of-plane shear modulus, G_{23}, can be also calculated assuming that the lamina is transversally isotropic [17]. This kind of models presents good predictions for E_1 and ν_{12}, but the estimations for associations in parallel are poor due to perturbations on the stress and strain fields related to stress concentration around the inclusions [17].

Other ROM-based models have been proposed to improve results for E_2, G_{12} and G_{23}. Among these models, the most popular are Halpin–Tsai [22] and Chamis [23] models. Recently, Vignoli et al. [5, 17] proposed a modified version of ROM (VSPK – authors initials) that presents a better agreement with experimental data. The main drawback of these models is the requirement of calibration parameters.

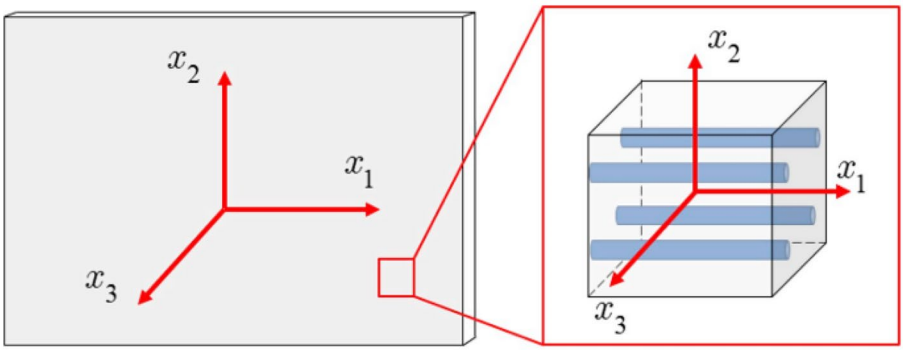

Fig. 1 Coordinate system for composite material properties

Huang et al. [24] developed a novel model assuming square symmetry of the unit cell and octagonal geometry of fibers. The load distribution analysis considers only strength of materials hypothesis for elements associated in series or in parallel, but a considerable improvement is observed comparing with the traditional ROM using a simplified geometry. Verma et al. [25] proposed a modeling approach considering a square symmetry of the unit cell and a circular fiber. Transversal load is of concern to evaluate the matrix damage. However, the expressions for effective elastic properties have not been derived.

Regarding the models based on the theory of elasticity, the asymptotic homogenization method is a rigorous mathematical modeling for periodic composites [26], presenting the closest estimation when compared with the experimental data [17]. Kalamkarov [27] presented an analytical solution for the effective elastic properties considering square symmetry of the unit cell and isotropic constituents. Later, it was generalized for transversally isotropic fibers [28] and simplified closed-form expressions with truncated series was proposed by Castillero et al. [29]. The classical Mori–Tanaka study [30], the influence of fiber orientation [31, 32], the fatigue life estimations [33] are additional examples of approaches developed based on the theory of elasticity. The large number of equations and the requirement of infinite series are the shortcoming for the applications of the models based on the theory of elasticity.

Finally, the third analytical approach to estimate the effective elastic properties of unidirectional composite is based on the empirical observation that the trace of the stiffness matrix is constant, which makes this a material property that can be used to estimate the other effective properties [1, 34]. It was initially proposed for carbon fiber laminae, but some investigations about its applications for other fibers have been performed [35]. A trial for theoretical basis discussion was carried out by Arteiro et al. [36] and several engineering applications have been proposed [37]. A comparison among trace theory with other micromechanical models is discussed by Vignoli et al. [20] showing a good estimation of this approach.

This paper proposes a novel model to estimate the effective elastic properties of unidirectional composites with circular cross section fibers: VSPKc. The proposed approach is an original ROM-based model based on the fiber and matrix properties, considering a unit cell with a specific fiber cross section geometry. The main advantage of this approach is that it does not require calibrated parameters, being associated with a reduced number of equations. Predictions of the proposed model are compared with experimental data and other alternative approaches as the classical ROM, the model assuming fiber octagonal geometry [24] and finite element simulations. Results show that the VSPKc model presents the best predictions using simpler equations.

2 VSPKc Model

The proposed VSPKc model is based on the Rule of Mixtures (ROM) and establishes closed-form expressions to calculate the effective elastic properties of unidirectional laminae. The idea is to define a square unit cell with a circular cross section fiber embedded in the matrix, following a similar strategy of presented in references [24, 25].

The VSPKc model is based on the unit cell presented in the Fig. 2 that shows the fiber's diameter D, the unit cell length in x_2 and x_3 equal to L, the unit cell length in x_1 equal to Δx_1, the fiber volume fraction is $V_f = \pi D^2/4L$, and consequently, $D/L = 2\sqrt{V_f/\pi}$.

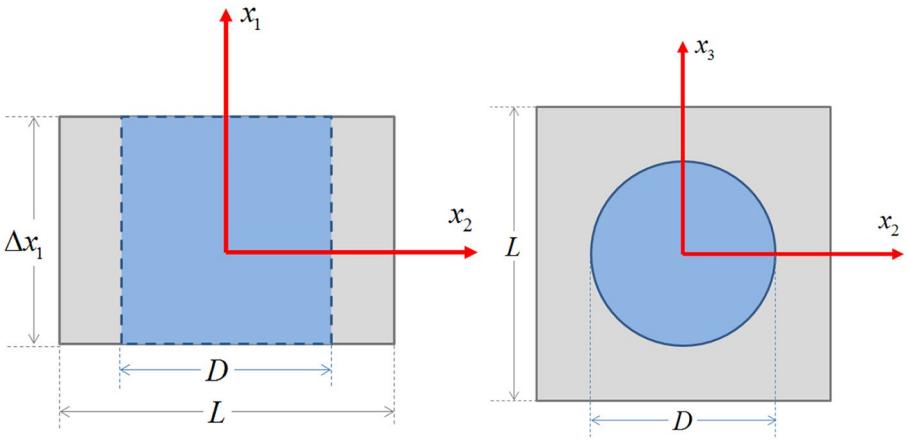

Fig. 2 Unit cell with square symmetry and circular fiber

Regarding the properties E_1 and ν_{12}, both fiber and matrix present the same strain and therefore, it can be assumed to be elements in parallel association that results in the classical ROM estimation described on following equations [17]:

$$E_1 = E_1^f V_f + E^m(1 - V_f) \tag{1}$$

$$\nu_{12} = \nu_{12}^f V_f + \nu^m(1 - V_f) \tag{2}$$

where E_1^f is the fiber longitudinal elastic modulus, ν_{12}^f is the fiber in-plane Poisson's ratio, E^m is the matrix elastic modulus, ν^m is the matrix Poisson's ratio and V_f is the fiber volume fraction.

2.1 Tranversal Elastic Modulus E_2

The determination of the transversal elastic modulus consider a transversal load on the unit cell, as presented in the Fig. 3. The unit cell is split into two regions: (*i*) only matrix; (*ii*) matrix and fiber. The proposed procedure yields a constitutive relation of the homogenized unit cell with the form $\langle\sigma_{22}\rangle = E_2\langle\varepsilon_{22}\rangle$, where $\langle\sigma_{22}\rangle$ and $\langle\varepsilon_{22}\rangle$ are the transversal stress and strain on the unit cell, respectively, and E_2 is the effective transversal elastic modulus to be derived. Considering that regions (*i*) and (*ii*) are parallel and the unit cell is symmetric, the equilibrium requirement can be expressed by

$$\langle\sigma_{22}\rangle = \frac{2}{L\Delta x_1}\left(\int_{D/2}^{L/2} \sigma_{22}^{(i)} dx_3 \Delta x_1 + \int_{0}^{D/2} \sigma_{22}^{(ii)} dx_3 \Delta x_1\right) \tag{3}$$

where $\sigma_{22}^{(i)}$ and $\sigma_{22}^{(ii)} = \sigma_{22}^{(ii)}(x_3)$ are the stresses in regions (*i*) and (*ii*), respectively.

For region (*i*), $\sigma_{22}^{(i)}$ can be assumed independent of x_3, since there is no fiber. The matrix constitutive relation can be applied to obtain

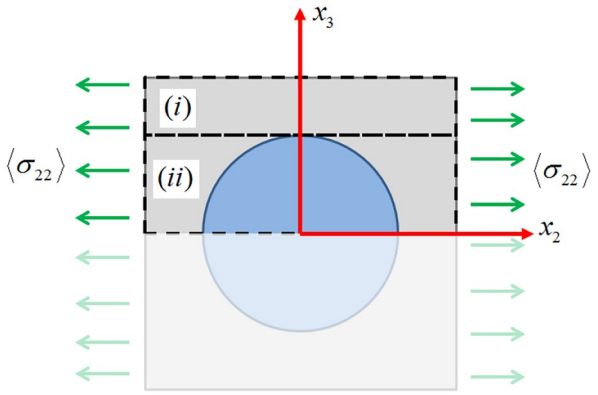

Fig. 3 Transversal load applied to the unit cell

$$\int_{D/2}^{L/2} \sigma_{22}^{(i)} dx_3 = \int_{D/2}^{L/2} E^m \varepsilon_{22}^{(i)} dx_3 = \frac{1}{2} E^m \varepsilon_{22}^{(i)} (L - D) \tag{4}$$

In region (ii), the stress $\sigma_{22}^{(ii)}$ is not independent of x_3, since matrix and fiber constitutive relations are necessary. First, consider the infinitesimal element shown in the Fig. 4. Assuming stress, σ_{22}^*, and strain, ε_{22}^*, it is desirable to obtain the effective elastic modulus E_2^* to define the constitutive relation $\sigma_{22}^* = E_2^* \varepsilon_{22}^*$. Since fiber and matrix are in series, the equilibrium requirement and geometrical compatibility are defined as follows:

$$\sigma_{22}^* = \sigma_{22}^m = \sigma_{22}^f \tag{5}$$

$$\varepsilon_{22}^* L = \varepsilon_{22}^m (L - D\cos\theta) + \varepsilon_{22}^f D\cos\theta \tag{6}$$

Defining the fiber volume fraction inside this infinitesimal element by $V_f^* = (D/L)\cos\theta = 2\sqrt{V_f/\pi}\cos\theta$, Eq. (5) can be rewritten as

$$\varepsilon_{22}^* = \varepsilon_{22}^m (1 - V_f^*) + \varepsilon_{22}^f V_f^* \tag{7}$$

Substituting the constitutive relations $\sigma_{22}^* = E_2^* \varepsilon_{22}^*$, $\sigma_{22}^f = E_2^f \varepsilon_{22}^f$ and $\sigma_{22}^m = E^m \varepsilon_{22}^m$ into Eq. (7),

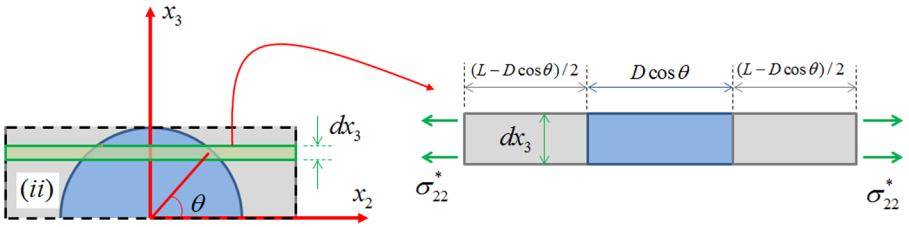

Fig. 4 Infinitesimal element of part (ii)

$$\frac{\sigma_{22}^{*}}{E_2^{*}} = \frac{\sigma_{22}^{m}}{E^{m}}(1 - V_f^{*}) + \frac{\sigma_{22}^{f}}{E_2^{f}} V_f^{*} \tag{8}$$

Using Eq. (5) and the definition $V_f^{*} = (D/L)\cos\theta = 2\sqrt{V_f/\pi}\cos\theta$, the effective elastic modulus of this infinitesimal element becomes

$$\frac{\sigma_{22}^{*}}{E_2^{*}} = \frac{\sigma_{22}^{m}}{E_2^{m}}\left(1 - V_f^{*}\right) + \frac{\sigma_{22}^{f}}{E_2^{f}} V_f^{*} \tag{9}$$

Note that Eq. (9) is different from the classical ROM formula since the term $V_f^{*} = 2\sqrt{V_f/\pi}\cos\theta$ appears instead of V_f in the classical ROM formula. In other words, the effective property of each infinitesimal region (*ii*), as represented in Fig. 4, is similar to the effective property estimated by the ROM where fiber and matrix are modeled as elements is series.

Once E_2^{*} is obtained, the stress integral of region (*ii*) can be expressed by

$$\int_0^{D/2} \sigma_{22}^{(ii)} dx_3 = \int_0^{D/2} E_2^{*}\varepsilon_{22}^{(ii)} dx_3 = E^{m}\varepsilon_{22}^{(ii)} \int_0^{D/2} \left\{ \frac{1}{1 + 2[(E^{m}/E_2^{f}) - 1]\sqrt{V_f/\pi}\cos\ \theta} \right\} dx_3 \tag{10}$$

Based on Fig. 4, $x_3 = (D/2)\sin\theta$ and $dx_3 = (D/2)\cos\theta d\theta$. Hence

$$\int_0^{D/2} \sigma_{22}^{(ii)} dx_3 = E^{m}\varepsilon_{22}^{(ii)} \frac{D}{2} \int_0^{\pi/2} \left\{ \frac{\cos\ \theta}{1 + a_{22}\cos\ \theta} \right\} d\theta \tag{11}$$

where $a_{22} = 2[(E^{m}/E_2^{f}) - 1]\sqrt{V_f/\pi}$ is denoted for the sake of simplicity. The integral presented in Eq. (11) is calculated by using MATLAB and the following expression is derived:

$$\int_0^{D/2} \sigma_{22}^{(ii)} dx_3 = E^{m}\sigma_{22}^{(ii)} \frac{D}{2} \left\{ \frac{\pi}{2a_{22}} - \frac{\ln\left[a_{22} + \sqrt{{a_{22}}^2 - 1}\right]}{a_{22}\sqrt{{a_{22}}^2 - 1}} \right\} \tag{12}$$

Substituting Eqs. (4) and (12) into Eq. (3) and assuming that $\langle\varepsilon_{22}\rangle = \varepsilon_{22}^{(i)} = \varepsilon_{22}^{(ii)}$ by geometrical compatibility, the following closed-form formula for the effective transversal modulus E_2 is obtained:

$$E_2 = E^{m}\left\{ 1 + 2\sqrt{\frac{V_f}{\pi}}\left[\frac{\pi}{2a_{22}} - \frac{\ln\left(a_{22} + \sqrt{{a_{22}}^2 - 1}\right)}{a_{22}\sqrt{{a_{22}}^2 - 1}} - 1 \right] \right\} \tag{13}$$

where $a_{22} = 2\left[\left(E^{m}/E_2^{f}\right) - 1\right]\sqrt{V_f/\pi}$.

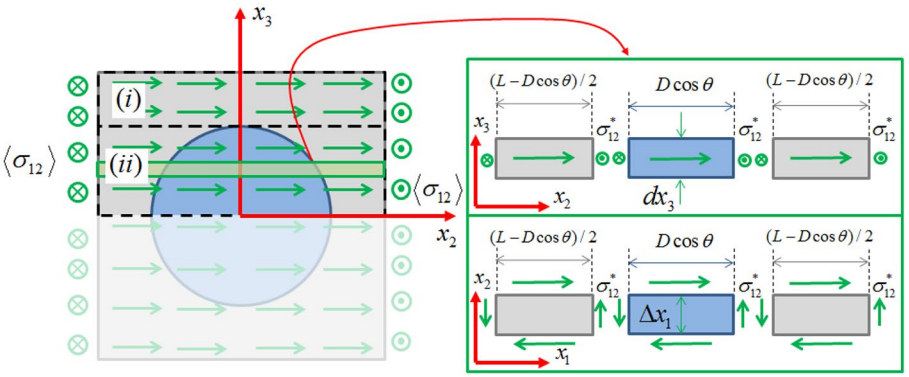

Fig. 5 In-plane shear load applied to the unit cell

2.2 In-plane Shear Modulus G_{12}

The estimation of the in-plane shear modulus is based on unit cell depicted in Fig. 5. The objective is to obtain an effective constitutive model to relate in-plane shear stress with the in-plane shear strain: $\langle\sigma_{12}\rangle = 2G_{12}\langle\varepsilon_{12}\rangle$. Based on Fig. 5, the equilibrium requirement of the face $A_1 = L^2$, perpendicular to $x_2 - x_3$ plane, is defined by

$$\langle\sigma_{12}\rangle = \frac{2}{L^2}\left(\int_{D/2}^{L/2}\sigma_{12}^{(i)}dx_3L + \int_{0}^{D/2}\sigma_{12}^{(ii)}dx_3L\right) \tag{14}$$

The integral of shear stress in region (i), where there is only matrix, is

$$\int_{D/2}^{L/2}\sigma_{12}^{(i)}dx_3 = \int_{D/2}^{L/2}2G^m\varepsilon_{12}^{(i)}dx_3 = G^m\varepsilon_{12}^{(i)}(L-D) \tag{15}$$

The following expression is obtained from a similar procedure to the one used for the effective transversal elastic modulus considering the infinitesimal region showed in Fig. 5:

$$G_{12}^* = G^m\left\{\frac{1}{1+2[(G^m/G_{12}^f)-1]\sqrt{V_f/\pi}\cos\theta}\right\} \tag{16}$$

Hence, the integral of region (ii) in Eq. (14) is

$$\int_{0}^{D/2}\sigma_{12}^{(ii)}dx_3 = \int_{0}^{D/2}2G_{12}^*\varepsilon_{12}^{(ii)}dx_3 = G^m\varepsilon_{12}^{(ii)}D\int_{0}^{\pi/2}\left\{\frac{\cos\theta}{1+a_{12}\cos\theta}\right\}d\theta, \tag{17}$$

where $a_{12} = 2\left[\left(G^m/G_{12}^f\right)-1\right]\sqrt{V_f/\pi}$. Note that this integral is similar to the one discussed in Eq. (11). Using the same symbolic solution, Eq. (17) can be rewritten as follows:

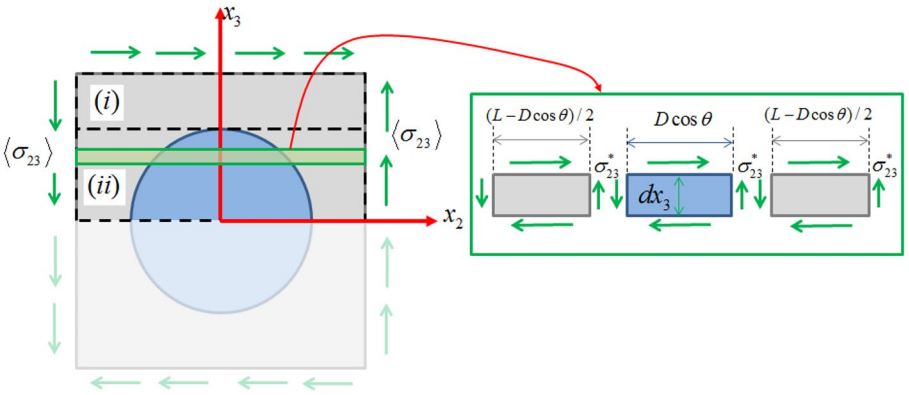

Fig. 6 Out-of-plane shear load applied to the unit cell

$$\int_0^{D/2} \sigma_{12}^{(ii)} dx_3 = G^m \varepsilon_{12}^{(ii)} D \left\{ \frac{\pi}{2a_{12}} - \frac{\ln\left[a_{12} + \sqrt{{a_{12}}^2 - 1}\right]}{a_{12}\sqrt{{a_{12}}^2 - 1}} \right\} \tag{18}$$

Considering that regions (i) and (ii) are parallel, $\langle\varepsilon_{12}\rangle = \varepsilon_{12}^{(i)} = \varepsilon_{12}^{(ii)}$. Using this compatibility condition and substituting Eqs. (15) and (18) into the Eq. (14), the following formula for the effective in-plane shear modulus G_{12} is derived:

$$G_{12} = G^m \left\{ 1 + 2\sqrt{\frac{V_f}{\pi}} \left[\frac{\pi}{2a_{12}} - \frac{\ln\left(a_{12} + \sqrt{a_{12}^2 - 1}\right)}{a_{12}\sqrt{a_{12}^2 - 1}} - 1 \right] \right\}, \tag{19}$$

where $a_{12} = 2\left[\left(G^m/G_{12}^f\right) - 1\right]\sqrt{V_f/\pi}$.

2.3 Out-of-plane Shear Modulus G_{23}

Out-of-plane shear modulus G_{23} is now in focus considering an out-of-plane load to establish a constitutive model $\langle\sigma_{23}\rangle = 2G_{23}\langle\varepsilon_{23}\rangle$. Comparing both shear loads presented in Figs. 5 and 6, it can be observed that they are similar. The main difference is the plane where the elements are assumed in parallel. The equilibrium requirement for out-of-plane shear load is defined as follows:

$$\langle\sigma_{23}\rangle = \frac{2}{L\Delta x_1}\left(\int_0^{D/2} \sigma_{23}^{(i)} dx_3 \Delta x_1 + \int_{D/2}^{L/2} \sigma_{23}^{(ii)} dx_3 \Delta x_1 \right) \tag{20}$$

Integrating the out-of-plane of shear stress in region (i) of Eq. (20), the following expression is obtained:

$$\int_{D/2}^{L/2} \sigma_{23}^{(i)} dx_3 = \int_{D/2}^{L/2} 2G^m \varepsilon_{23}^{(i)} dx_3 = G^m \sigma_{23}^{(i)} (L - D) \tag{21}$$

By assuming elements in series at the infinitesimal part illustrated in Fig. 6 and using the previously derived results, the effective out-of-plane shear modulus of each infinitesimal element in region (*ii*) is defined by

$$G_{23}^{*} = G^m \left\{ \frac{1}{1 + 2[(G^m/G_{23}^f) - 1]\sqrt{V_f/\pi}\cos\ \theta} \right\} \tag{22}$$

Once the effective constitutive relation in region (*ii*) is obtained, the stress integral in this region is computed by

$$\int_0^{D/2} \sigma_{23}^{(ii)} dx_3 = \int_0^{D/2} 2G_{23}^{*} \varepsilon_{23}^{(ii)} dx_3 = G^m \sigma_{23}^{(ii)} D \int_0^{\pi/2} \left\{ \frac{\cos\theta}{1 + a_{23}\cos\theta} \right\} \tag{23}$$

where $a_{23} = 2[(G^m/G_{23}^f) - 1]\sqrt{V_f/\pi}$. This integral is same as in Eqs. (11) and (17). Consequently,

$$\int_0^{D/2} \sigma_{23}^{(ii)} dx_3 = G^m \sigma_{23}^{(ii)} D \left\{ \frac{\pi}{2a_{23}} - \frac{\ln\left[a_{23} + \sqrt{{a_{23}}^2 - 1}\right]}{a_{23}\sqrt{{a_{23}}^2 - 1}} \right\} \tag{24}$$

Since regions (*i*) and (*ii*) are parallel, it is considered $\langle \varepsilon_{23} \rangle = \varepsilon_{23}^{(i)} = \varepsilon_{23}^{(ii)}$. By using Eqs. (20), (21) and (24), the following formula for the effective out-of-plane shear modulus G_{23} is derived:

$$G_{23} = G^m \left\{ 1 + 2\sqrt{\frac{V_f}{\pi}} \left[\frac{\pi}{2a_{23}} - \frac{\ln\left(a_{23} + \sqrt{a_{23}^2 - 1}\right)}{a_{23}\sqrt{a_{23}^2 - 1}} - 1 \right] \right\}, \tag{25}$$

where $a_{23} = 2[(G^m/G_{23}^f) - 1]\sqrt{V_f/\pi}$.

The novel VSPKc model is now completely formulated being described by Eqs. (1), (2), (13), (19), (25) and equations to compute a_{22}, a_{12} and a_{23}. This is a simple set of explicit analytical formulas that allows calculation of the 3D effective elastic properties of the unidirectional composite with circular fibers.

Table 1 Number of elements and nodes for FEM simulations

V_f	0.1	0.2	0.3	0.4	0.5	0.6	0.7
Elements	8960	6560	5760	5440	5280	4480	14925
Nodes	63923	47123	41523	39283	38163	32563	106728

3 Finite Element Method

The finite element method (FEM) model is built by considering the same essential hypothesis of the analytical model: composite behavior is based on the unit cell. Therefore, FEM model considers unit cells based on the fiber volume fraction. Ansys software is employed considering a quadratic and three-dimensional element: SOLID186. The unit cell is built considering the same fiber diameter and hence, different fiber volume fraction is represented by different unit cell size. Fiber and matrix are assumed to be perfectly bonded and the multi-point constraint formulation is applied. Seven situations are analyzed, being represented by different fiber volume fractions V_f: 0.1, 0.2, 0.3, 0.4, 0.5, 0.6, 0.7. Fiber diameter D and cell size Δx_1 are kept constants (see Fig. 2), $L = \sqrt{\pi D^2}/4V_f$. Table 1 presents details about the meshes obtained after a convergence analysis.

Periodic boundary conditions are imposed, being mathematically expressed by

$$U_i^{(J+)} - U_i^{(J-)} = \lambda_i^{(J)} \tag{26}$$

where $\lambda_1^{(J)}$ is a constant parameter that represents the difference between displacements of faces $J+$ and $_J-$ in i direction, $U_i^{(J+)}$ and $U_i^{(J-)}$, respectively [38].

The imposed periodic boundary conditions are associated with a force reaction. Three simulations are required to compute the five composite effective elastic properties for each V_f, as represented by the columns in Table 2. For instance, for the first column $U_1^{(1+)} = \lambda_1^{(1)}$ is the unique non-null displacement applied, $R_1^{(1)}$ and are computed by the FEM. Note that the reactions are directly obtained by solving the FEM equation once the displacement is imposed. Based on these quantities, the unique non-null strain component $\langle \varepsilon_{11} \rangle$ and the

Table 2 Periodic boundary conditions

Applied Displacements	$U_1^{(1+)} = \lambda_1^{(1)}$	$U_2^{(2+)} = \lambda_2^{(2)}$	$U_1^{(2+)} = \lambda_1^{(2)}$
Null Displacements	$U_1^{(1-)}$, $U_2^{(2+)}, U_2^{(2-)}$, $U_3^{(3+)}, U_3^{(3-)}$	$U_1^{(1+)}, U_1^{(1-)}$, $U_2^{(2-)}$, $U_3^{(3+)}, U_3^{(3-)}$	$U_2^{(1+)}, U_2^{(1-)}, U_3^{(1+)}, U_3^{(1-)}$, $U_1^{(2-)}, U_2^{(2+)}, U_2^{(2-)}, U_3^{(2+)}, U_3^{(2-)}$, $U_2^{(3+)}, U_2^{(3-)}, U_3^{(3+)}, U_3^{(3-)}$
Strains	$\langle \varepsilon_{11} \rangle = \frac{\lambda_1^{(1)}}{\Delta x_1}$	$\langle \varepsilon_{22} \rangle = \frac{\lambda_2^{(2)}}{L}$	$\langle \varepsilon_{12} \rangle = \frac{\lambda_1^{(2)}}{2L}$
Stresses	$\langle \sigma_{11} \rangle = \frac{R_1^{(1)}}{L^2}$	$\langle \sigma_{22} \rangle = \frac{R_2^{(2)}}{\Delta x_1 L}$	$\langle \sigma_{12} \rangle = \frac{R_1^{(2)}}{\Delta x_1 L}$
	$\langle \sigma_{22} \rangle = \frac{R_2^{(2)}}{\Delta x_1 L}$	$\langle \sigma_{33} \rangle = \frac{R_3^{(3)}}{\Delta x_1 L}$	
Effective Properties	$C_{11} = \frac{\langle \sigma_{11} \rangle}{\langle \varepsilon_{11} \rangle}$	$C_{22} = \frac{\langle \sigma_{22} \rangle}{\langle \varepsilon_{22} \rangle}$	$C_{66} = \frac{\langle \sigma_{12} \rangle}{2\langle \varepsilon_{12} \rangle}$
	$C_{12} = \frac{\langle \sigma_{22} \rangle}{\langle \varepsilon_{11} \rangle}$	$C_{23} = \frac{\langle \sigma_{33} \rangle}{\langle \varepsilon_{22} \rangle}$	

stress components and $\langle \sigma_{22} \rangle$ are obtained. Therefore, elastic matrix elements and C_{12} can be evaluated. Analogous analyses are developed for the other columns.

By assuming a transversally isotropic homogenized material, the composite effective stiffness matrix is defined by

$$C = \begin{bmatrix} C_{11} & C_{12} & C_{12} & 0 & 0 & 0 \\ C_{12} & C_{22} & C_{23} & 0 & 0 & 0 \\ C_{12} & C_{23} & C_{33} & 0 & 0 & 0 \\ 0 & 0 & 0 & C_{44} & 0 & 0 \\ 0 & 0 & 0 & 0 & C_{66} & 0 \\ 0 & 0 & 0 & 0 & 0 & C_{66} \end{bmatrix} \tag{27}$$

where $C_{44} = \left(C_{22} - C_{23}\right)/2$.

Finally, by evaluating the compliance matrix, $\mathbf{S} = \mathbf{C}^{-1}$, the composite effective elastic properties are obtained as follows,

$$E_1 = \frac{1}{S_{11}} \tag{28}$$

$$E_2 = \frac{1}{S_{22}} \tag{29}$$

$$\nu_{12} = -E_1 S_{12} \tag{30}$$

$$G_{12} = \frac{1}{S_{66}} \tag{31}$$

$$G_{23} = \frac{1}{S_{44}} \tag{32}$$

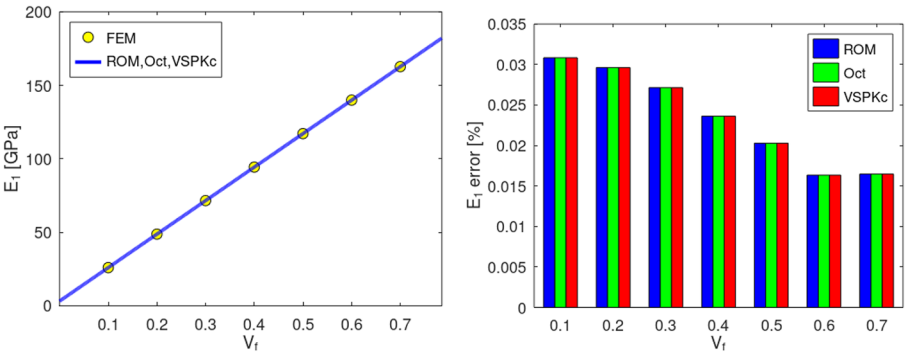

Fig. 7 Comparison between analytical estimations and FEM results for E_1: (**a**) influence of V_f; (**b**) absolute error

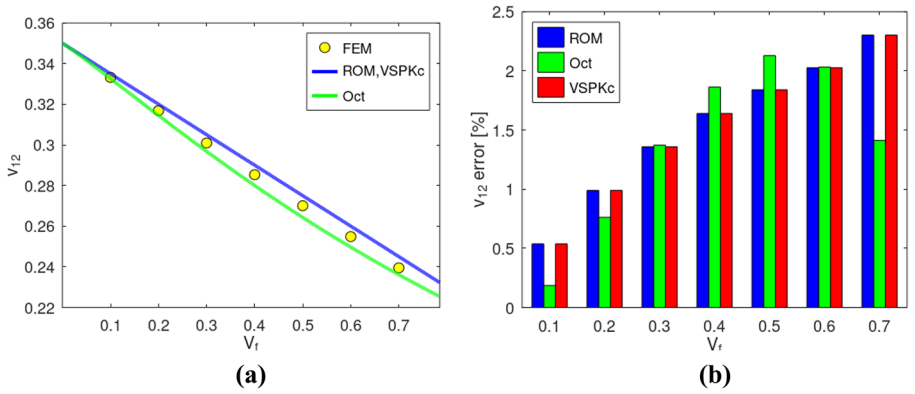

Fig. 8 Comparison between analytical estimations and FEM results for v_{12}: (**a**) influence of V_f; (**b**) absolute error

4 Results and Discussion

Results of the proposed VSPKc model are discussed by comparing its results with with two alternative models available in the literature: ROM [21] and octagonal fibers model (Oct) [24]. Finite element method (FEM) is employed for model verification, being assumed to be a reference. In addition, a set of 126 compiled experimental data for carbon and glass fibers and epoxy matrices [39–52] are employed for the comparison with the analytical estimations.

A composite made by an epoxy matrix with $E^m = 3.2$GPa, $\nu^m = 0.35$ and transversely isotropic carbon fibers with $E_1^f = 231$GPa, $E_1^f = 15$GPa, $G_{12}^f = 15$GPa, $G_{23}^f = 7$GPa and $\nu_{12}^f = 0.2$GPa is considered [35]. Figure 7 shows the comparison of analytical models with FEM results for E_1. The three analytical models use the same equation for E_1, Eq. (1). Results indicate that the error tends to zero and a simple equation is sufuciently acurate to estimate this property [17]. Results for ν_{12} are presented in Fig. 8 and, despite

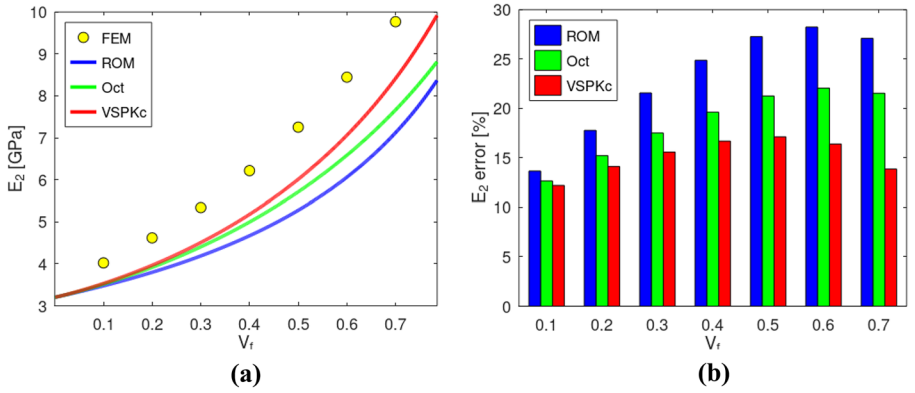

Fig. 9 Comparison between analytical estimations and FEM results for E_1: (**a**) influence of V_f; (**b**) absolute error

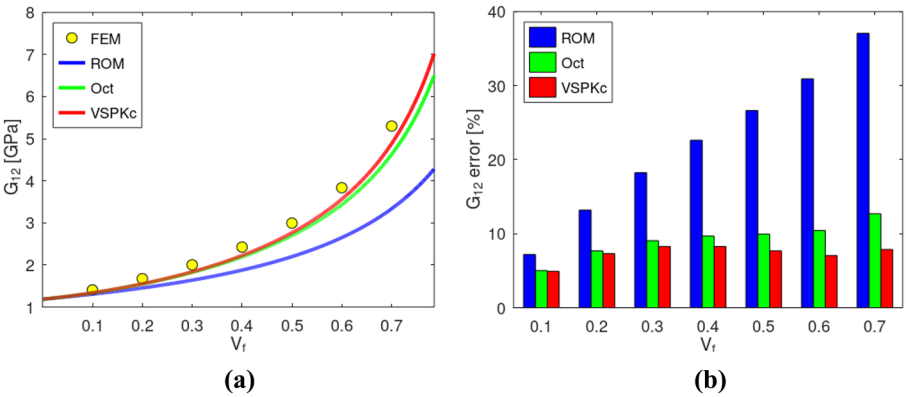

Fig. 10 Comparison between analytical estimations and FEM results for G_{12}: (**a**) influence of V_f; (**b**) absolute error

Oct model uses an equation slightly different than Eq. (2), no considerable improvement is achieved.

Figure 9 presents results for E_2 showing that VSPKc has the best predicions compared with FEM. Results of the classical ROM presents error ranges between 13.6% and 28.2%; Oct model presents error ranges between 12.7% and 22%; VSPKc error ranges are between 12.2% and 17.1%. Additionally, the error tends to increase when V_f for ROM, while a small variation is achieved for VSPKc.

Figure 10 presents results for G_{12} showing that the ROM has error ranges between 7.2% and 37.1%; Oct has error ranges between 5% and 12.7%; VSPKc presents error ranges between 4.9% and 8.3%. Once again, VSPKc model has the best estimation for any V_f.

Figure 11 presents results for G_{23} showing that ROM estimations has error ranges between 17.4% and 37.6%; Oct presents error ranges between 2.8% and 16.2%; on the other hand, VSPKc has error ranges between 2.7% and 14%. Once again, VSPKc model

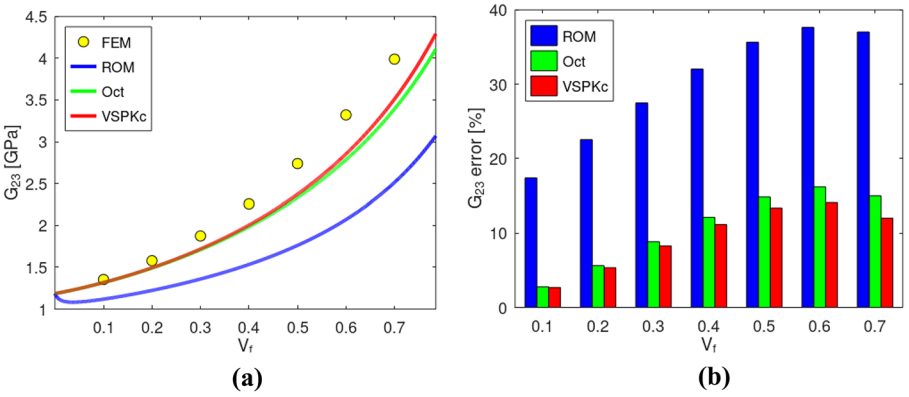

Fig. 11 Comparison between analytical estimations and FEM results for G_{23}: (**a**) influence of V_f; (**b**) absolute error

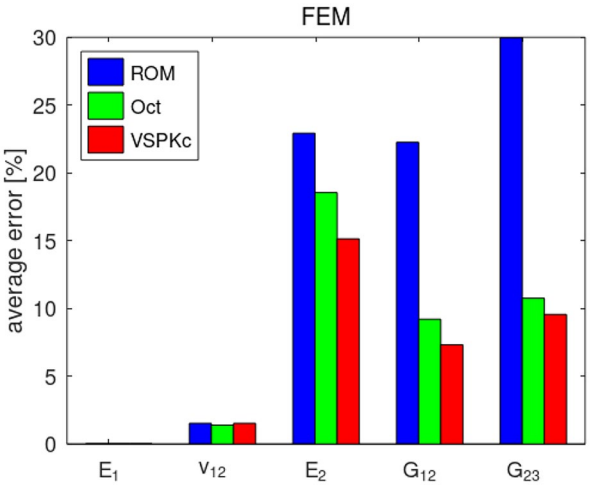

Fig. 12 Average error comparing analytical estimations with and FEM results

has the best estimation for any V_f and these results indicate a considerable estimation improvement due to the fiber's geometry consideration.

A summary of the comparison between analytical models and FEM is presented in Fig. 12 and the following conclusions can be highlighted:

i). the classical ROM estimations for E_1 and ν_{12}, see Eqs. (1) and (2), are very accurate;
ii). a considerable improvement is obtained when the fiber's geometry description is refined;
iii). VSPKc model obtained smaller errors than other analytical models for all properties, indicating a considerable modeling improvement;
iv). the average error is higher for E_2 than for G_{12} and G_{23} because the Poisson's effect is not considered on the analytical modeling.

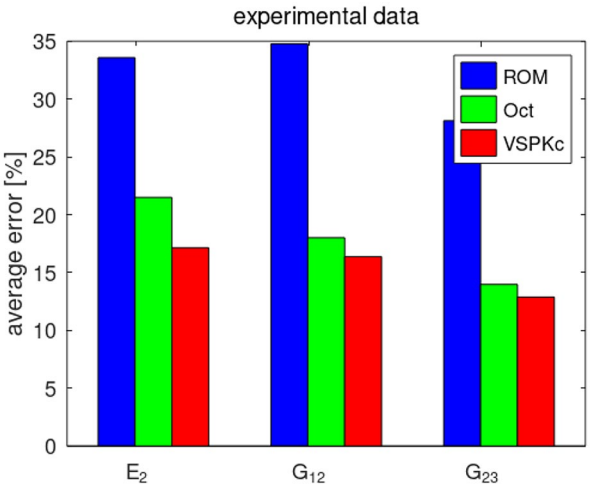

Fig. 13 Average errors for the effective properties E_2, G_{12} and G_{23} of the analytical models compared with the experimental data

A set of 126 compiled experimental results are now employed to verify the different models. This set has 54 data for E_2, 46 data for G_{12} and 26 data for G_{23}. For simplicity, only the estimations of E_2, G_{12} and G_{23} are compared since there is no considerable differences between the estimations of E_1 and v_{12} [17]. Figure 13 shows the comparison among the ROM, Oct, and VSPKc predictions. In the general sense, there is a clear trend due to the improvement of the analytical estimations, where VSPKc is the closest prediction, followed by Oct, and the worst predictions are the ones obtained by ROM. Specifically, the novel VSPKc model presents the following average errors: 12.9% for G_{23}, 16.4% for G_{12} and 17.1% for E_2. Once again, VSPKc has reliable estimations with a simple set of 8 equations without any calibration parameter.

5 Conclusions

This paper presents a novel ROM-based model to estimate the effective properties of elastic unidirectional composites with circular cross section fibers. The main advantage of the VSPKc model is that it is expressed by 8 explicit analytical formulas and does not require experimentally calibrate parameters. Results show the importance of accounting the fiber geometry in order to improve the accuracy of the effective properties, which is carried out assuming a square unit cell. The average errors between VSPKc estimations and FEM are 15.1% for E_2, 7.3% for G_{12} and 9.5% for G_{23}. Comparing with experimental data, VSPKc average errors are 17.1% for E_2, 16.3% for G_{12} and 12.85% for G_{23}. The comparison with either the FEM and experimental data highlights that VSPKc has closer estimations than other alternative analytical models (specifically, ROM and Oct).

Funding The authors would like to acknowledge the support of the Brazilian Research Agencies CNPq, CAPES, FAPERJ and the Natural Sciences and Engineering Research Council of Canada (NSERC).

Data Availability Data available on request.

References

1. Tsai, S.W., Melo, J.D.D.: An invariant-based theory of composites. Compos. Sci. Technol. **100**, 237–243 (2014)
2. Andrianov, I.V., Awrejcewicz, J., Danishevs'kyy, V.V.: Asymptotical mechanics of composites - modelling composites without FEM. Springer (2018)
3. Kalamkarov, A.L., Kolpakov, A.G.: Analysis, Design and Optimization of Composite Structure, 2nd edn. Wiley (1997)
4. Vignoli, L.L., Savi, M.A.: Multiscale Failure Analysis of Cylindrical Composite Pressure Vessel: A Parametric Study. Lat. Am. J. Solids. Struct. **15**, 1–20 (2018)
5. Vignoli, L.L., Savi, M.A., Pacheco, P.M.C.L., Kalamkarov, A.L.: Multiscale Approach to Predict Strength of Notched Composite Plates. Comp. Struct. **253**, 112827 (2020)
6. Vignoli, L.L., Kenedi, P.P., Mariano, M.J.B.: Exploring Thermography Technique to Validate Multiscale Procedure for Notched CFRP Plates. Compos. C. Open. Access. **7**, 100241 (2022)
7. Tsai, S.W.: Double–Double: New Family of Composite Laminates. AIAA. J. **59**(11), 4293–4305 (2021)
8. Kalamkarov, A.L., Andrianov, I., Starushenko, G.: Refinement of the Maxwell Formula for Fiber-Reinforced Composites. J. Multiscale. Model. **11**(1), 1950001 (2020)

9. Yousefi, S.R., Alshamsi, H.A., Amiri, O., Salavati-Niasari, M.: Synthesis, characterization and application of Co/Co3O4 nanocomposites as an effective photocatalyst for discoloration of organic dye contaminants in wastewater and antibacterial properties. J. Mol. Liq. **337**, 116405 (2021)
10. Yousefi, S.R., Sobhani, A., Salavati-Niasari, M.: A new nanocomposite superionic system (CdHgI4/HgI2): Synthesis, characterization and experimental investigation. Adv. Powder. Technol. **28**, 1258–1262 (2017)
11. Dinulovic, M., Rasuo, B.: Dielectric modeling of multiphase composites. Compos. Struct. **93**(12), 3209–3215 (2011)
12. Yousefi, S.R., Ghanbari, D., Salavati, N.M.: Hydrothermal Synthesis of Nickel Hydroxide Nanostructures and Flame Retardant Poly Vinyl Alcohol and Cellulose Acetate Nanocomposites. J. Nanostruct. **6**, 77–82 (2016)
13. Alam, A., Saha, G.C., Kalamkarov, A.L.: Micromechanical analysis of quantum dot-embedded smart nanocomposite materials. Compos. C. Open. Access. **3**, 100062 (2020)
14. Elnekhaily, S.A., Talreja, R.: Damage initiation in unidirectional fiber composites with different degrees of nonuniform fiber distribution. Compos. Sci. Technol. **155**, 22–32 (2018)
15. Benzarti, K., Cangemi, L., Maso, F.D.: Transverse properties of unidirectional glass/epoxy composites: influence of fibre surface treatments. Compos. A. **32**, 197–206 (2001)
16. Ramos, R.R., Medeiros, R., Díaz, R.G., Castillero, J.B., Otero, J.A., Tita, T.: Different approaches for calculating the effective elastic properties in composite materials under imperfect contact adherence. Compos. Struct. **99**, 264–275 (2013)
17. Vignoli, L.L., Savi, M.A., Pacheco, P.M.C.L., Kalamkarov, A.L.: Comparative analysis of micromechanical models for the elastic composite laminae. Compos. B. **174**, 106961 (2019)
18. Vignoli, L.L., Savi, M.A., Pacheco, P.M.C.L., Kalamkarov, A.L.: Micromechanical analysis of transversal strength of composite laminae. Compos. Struct. **250**, 112546 (2020)
19. Vignoli, L.L., Savi, M.A., Pacheco, P.M.C.L., Kalamkarov, A.L.: Micromechanical analysis of longitudinal and shear strength of composite laminae. J. Compos. Mater. **54**, 4853–4873 (2020)
20. Vignoli, L.L., Neto, R.M.C., Savi, M.A., Pacheco, P.M.C.L., Kalamkarov, A.L.: Trace Theory Applied to Composite Analysis: A Comparison with Micromechanical Models. Compos. Commun. **25**, 100715 (2021)
21. Jones, R.M.: Mechanics of composite materials, 2nd edn. Taylor & Francis (1999)
22. Halpin, J.C., Tsai, S.W.: Effects of environmental factors on composite materials, pp. 67–423. AFML-TR (1969)
23. Chamis, C.C., Abdi, F., Garg, M., Minnetyan, L., Baid, H., Huang, D., Housner, J., Talagani, F.: Micromechanics-based progressive failure analysis prediction for WWFE-III composite coupon test cases. J. Compos. Mater. **47**, 2695–2712 (2013)
24. Huang, Y., Cimini, C.A., Jr., Ha, S.K.: A micromechanical unit cell model with an octagonal fiber for continuous fiber reinforced composites. J. Compos. Mater. **54**, 4495–4513 (2020)
25. Verma, A., Vedantam, S., Akella, K., Sivakumar, S.M.: Micromechanics based analytical model for estimation of stress distribution and failure initiation in constituents of UDFRP composites subjected to transverse loading. Ann. Solid. Struct. Mech. **12**, 189–197 (2020)
26. Kalamkarov, A.L., Andrianov, I.V., Danishevs'kyy, V.V.: Asymptotic homogenization of composite materials and structures. Trans. ASME. Appl. Mech. Rev. **62**, 030802 (2009)
27. Kalamkarov, A.L.: Composite and Reinforced Elements of Construction. Wiley, N-Y (1992)
28. Ramos, R.R., Sabina, F.J., Díaz, R.G., Castillero, J.B.: Closed-form expressions for the effective coefficients of a fiber-reinforced composite with transversely isotropic constituents - I Elastic and square symmetry. Mech. Mater. **33**, 223–235 (2001)
29. Castillero, J.B., Díaz, R.G., Ramos, R.R., Sabina, F.J., Brenner, R.: Unified analytical formulae for the effective properties of periodic fibrous composites. Mater. Lett. **73**, 68–71 (2012)
30. Mori, T., Tanaka, K.T.: Average stress in matrix and average elastic energy of materials with misfitting inclusions. Acta. Metall. **21**, 571–574 (1973)
31. Kalamkarov, A.L., Liu, H.Q.: A new model for the multiphase fiber–matrix composite materials. Compos. B. Eng. **29**, 643–653 (1998)
32. Brighenti, R., Scorza, D.: A micro-mechanical model for statistically unidirectional and randomly distributed fibre-reinforced solids. Math. Mech. Solids. **17**, 876–893 (2012)
33. Brighenti, R., Carpinteri, A., Scorza, D.: Micromechanical crack growth-based fatigue damage in fibrous composites. Int. J. Fatigue. **82**, 98–109 (2016)
34. Tsai, S.W., Sharma, N., Arteiro, A., Roy, S., Rainsberger, B.: Composite grid/skin structures - Low weight/low cost design and manufacturing. Stanford University (2019)
35. Ha, S.K., Cimini, C.A., Jr.: Theory and validation of the master ply concept for invariant-based stiffness of composites. J. Compos. Mater. **52**, 1699–1708 (2018)

36. Arteiro, A., Pereira, L.F., Bessa, M.A., Furtado, C., Camanho, P.P.: A micro-mechanics perspective to the invariant-based approach to stiffness. Compos. Sci. Technol. **176**, 72–80 (2019)
37. Arteiro, A., Sharma, N., Melo, J.D.D., Ha, S.K., Miravete, A., Miyano, Y., Massard, T., Shah, P.D., Roy, S., Rainsberger, R., Rother, K., Cimini, C.A., Jr., Seng, J.M., Arakaki, F.K., Tay, T.E., Lee, W.I., Sihn, S., Springer, G.S., Roy, A., Riccio, A., Di Caprio, F., Shrivastava, S., Nettles, A.T., Catalanotti, G., Camanho, P.P., Seneviratne, W., Marques, A.T., Yang, H.T., Hahn, H.T.: A case for Tsai's Modulus, an invariant-based approach to stiffness. Compos. Struct. **252**, 112683 (2020)
38. Barbero, E.J.: Finite Element Analysis of Composite Materials. CRC Press (2008)
39. Kaddour, A.S., Hinton, M.J., Smith, P.A., Li, S.: The background to the third world-wide failure exercise. J. Compos. Mater. **47**, 2417–2426 (2013)
40. Kriz, R.D., Stinchcomb, W.W.: Elastic moduli of transversely isotropic graphite fibers and their composites. Exp. Mech. **19**, 41–49 (1979)
41. Tsai, S.W., Hahn, H.T.: Introduction to composite materials. Technomic (1980)
42. Soden, P.D., Hinton, M.J., Kaddour, A.S.: Lamina properties, lay-up configurations and loading conditions for a range of fibre-reinforced composite laminates. Compos. Sci. Technol. **58**, 1011–1022 (1998)
43. Bledzki, A.K., Kessler, A., Rikard, R., Chate, A.: Determination of elastic constants of glass/epoxy unidirectional laminates by the vibration testing of plates. Compos. Sci. Technol. **59**, 2015–2024 (1999)
44. Yim, J.H., Gillespie, J.W., Jr.: Damping characteristics of 0 and 90 AS4/3501-6 unidirectional laminates including the transverse shear effect. Compos. Struct. **50**, 217–225 (2000)
45. Huang, H., Talreja, R.: Effects of void geometry on elastic properties of unidirectional fiber reinforced composites. Compos. Sci. Technol. **65**, 1964–1981 (2005)
46. Camanho, P.P., Maimí, P., Davila, C.G.: Prediction of size effects in notched laminates using continuum damage mechanics. Compos. Sci. Technol. **67**, 2715–2727 (2007)
47. Lee, J., Soutis, C.: A study on the compressive strength of thick carbon fibre-epoxy laminates. Compos. Sci. Technol. **67**, 2015–2026 (2007)
48. Benzarti, K., Cangemi, L., Maso, F.D.: Transverse properties of unidirectional glass/epoxy composites: influence of fibre surface treatments. Compos. A. **2001**(32), 197–206 (2001)
49. Kaddour, A.S., Hinton, M.J.: Input data for test cases used in benchmarking triaxial failure theories of composites. J. Compos. Mater. **46**, 2295–2312 (2012)
50. Schaefer, J.D., Werner, B.T., Daniel, I.M.: Strain-rate-dependent failure of a toughened matrix composite. Exp. Mech. **54**, 1111–1120 (2014)
51. Li, W., Cai, H., Zheng, J.: Characterization of strength of carbon fiber reinforced polymer composite based on micromechanics. Polym. Polym. Compos. **22**, 2 (2014)
52. Huang, Z.M.: Micromechanical prediction of ultimate strength of transversely isotropic fibrous composites. Int. J. Solids. Struct. **38**, 4147–4172 (2001)

Publisher's Note Springer Nature remains neutral with regard to jurisdictional claims in published maps and institutional affiliations.